Ferromagnetic insulating epitaxially strained La$_2$NiMnO$_6$ thin films grown by sputter deposition

View Online   Export Citation   CrossMark

G. De Luca,[1,a] (ID) J. Spring,[1] U. Bashir,[1] M. Campanini,[2] (ID) R. Totani,[1,b] (ID) C. Dominguez,[3] (ID) A. Zakharova,[4] (ID)
M. Döbeli,[5] (ID) T. Greber,[1] (ID) M. D. Rossell,[2] (ID) C. Piamonteze,[4] (ID) and M. Gibert[1] (ID)

AFFILIATIONS

[1] Physik-Institut, University of Zurich, Winterthurerstrasse 190, CH-8057 Zurich, Switzerland
[2] Electron Microscopy Center, Empa, Swiss Federal Laboratories for Materials Science and Technology, Überlandstrasse 129, CH-8600 Dübendorf, Switzerland
[3] Department of Quantum Matter Physics, University of Geneva, Quai E.-Ansermet 24, CH-1211 Geneva, Switzerland
[4] Swiss Light Source, Paul Scherrer Institut, CH-5232 Villigen PSI, Switzerland
[5] Laboratory of Ion Beam Physics, ETH Zürich, Otto-Stern-Weg 5, CH-8093 Zürich, Switzerland

[a] Author to whom correspondence should be addressed: deluca@physik.uzh.ch
[b] Current address: CNR-ISM, Elettra Sincrotrone Trieste, I-34149 Basovizza, Italy.

ABSTRACT

The field of oxide spintronics can strongly benefit from the establishment of ferromagnetic insulators with near room-temperature Curie temperature. Here, we investigate the structural, electronic, and magnetic properties of epitaxially strained thin films of the double perovskite La$_2$NiMnO$_6$ (LNMO) grown by off-axis radio-frequency magnetron sputtering. We find that the films retain insulating behavior and a bulk-like Curie temperature in the order of 280 K independently of the epitaxial strain conditions. These results suggest a prospective implementation of LNMO films in multi-layer device architectures where a high-temperature ferromagnetic insulating state is a prerequisite.

I. INTRODUCTION

The development of robust and easy to integrate ferromagnetic insulators (FMIs) is a crucial objective for the progress of next-generation dissipationless oxide spintronic devices.[1–3] Unfortunately, the coexistence of these features is rarely found in nature, mainly because the electrons that mediate FM interactions are typically itinerant.[4] Transition metal oxides, and in particular perovskite-based systems, have been widely studied in the last few decades because of the vast combination of functionalities that can be hosted in a relatively simple structure.[5,6] Recent efforts, indeed, have demonstrated that doping, off-stoichiometry, epitaxial strain, and interface engineering are examples of feasible strategies to obtain a FMI behavior in perovskite oxide heterostructures.[7–11]

These exotic states are, however, in competition with a metallic one, suggesting that their adoption in a device architecture could be fragile. In this perspective, it would be more favorable if the nature of the FM interaction was intrinsically insulating.

One possible route to realize this state is provided by double perovskites (DPs). These are compounds characterized by a specific substitution in the ABO$_3$ prototypical perovskite unit cell where exactly half of the A- (B-)site cations are replaced with another cation A$'$ (B$'$). When these atoms follow a specific long-range order (rock-salt, layered, or columnar), the resulting structure is known as A-(B-) site ordered DP and the new compound is characterized by the chemical formula AA$'$B$_2$O$_6$ (A$_2$BB$'$O$_6$).[12] A sketch of a B-site rock-salt-ordered DP structure with the pseudocubic cell overlaid in blue is shown in Fig. 1(a). Due to their structure being similar
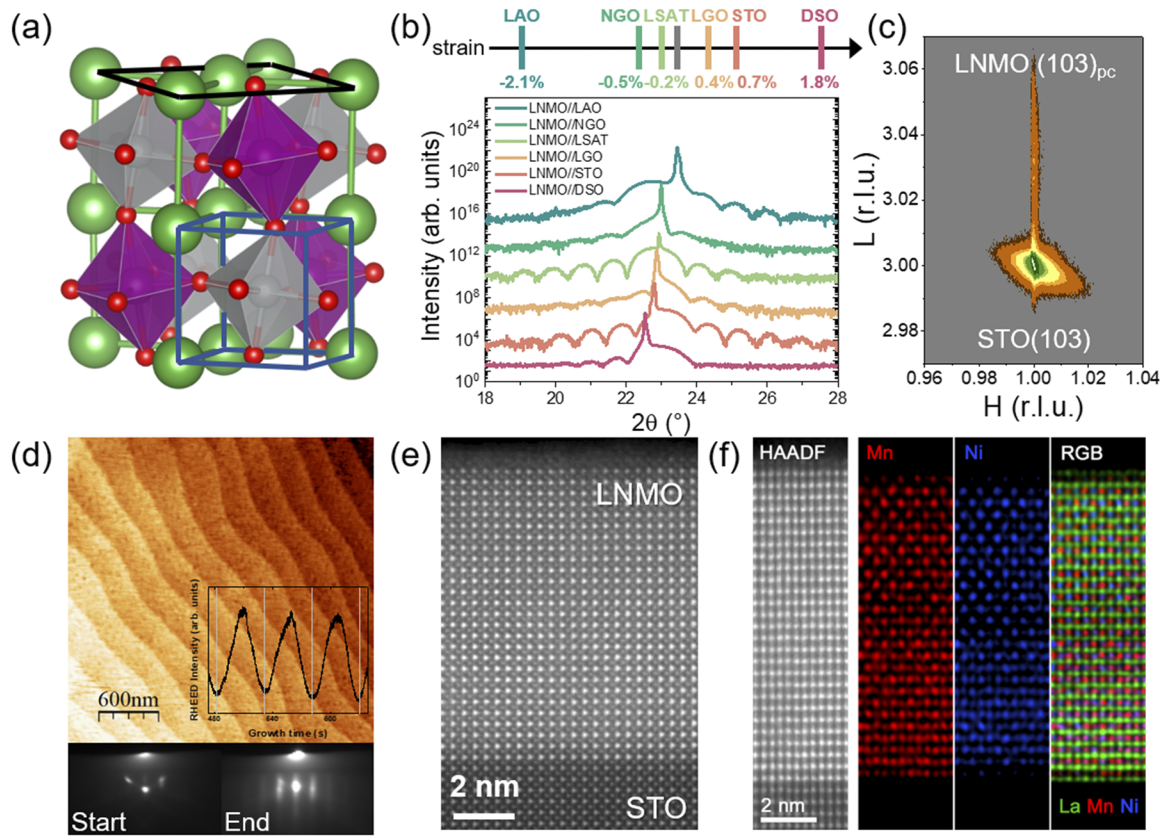
FIG. 1. Structural characterization of epitaxially strained LNMO thin films. (a) Schematic of a DP unit cell. The A-cation is shown in green, while the oxygen ions are shown in red. The two different B-cations and their corresponding octahedra are shown in gray and purple. The base of the orthorhombic (monoclinic) structure is defined by the black square. The pc unit cell is shown in blue. (b) X-ray θ–2θ diffractograms of various LNMO films around the $(001)_{pc}$ planes of the respective substrates. Fringes are due to finite size effects and have been used to evaluate the film thickness, that is, in the order of 30 uc. Different datasets are vertically shifted for better visibility. On top, the nominal strain exerted on the epitaxial LNMO films by the distinct substrates is highlighted. (c) Reciprocal space map around the $(103)_{STO}$ diffraction condition certifies the fully strained state of the LNMO film. (d) Top panel: surface topography of a representative LNMO//STO film as obtained by AFM. Inset: detail of the intensity oscillations of the RHEED specular spot. The gray lines correspond to a period of 49 s. Left (right) bottom panel: RHEED diffraction patterns before (after) the growth of a 30 uc LNMO//STO film. (e) The HAADF-STEM image along the $[100]_{STO}$ zone axis shows a high crystalline quality of the film and the absence of parasitic defects. (f) The HAADF-STEM image and the corresponding EDX elemental maps of Mn and Ni along the $[110]_{STO}$ zone axis show the rock-salt ordering of the Mn and Ni cations. The RGB image (red = Mn, green = La, blue = Ni) facilitates the observation of the B and B' cation ordering.

to standard perovskites, these compounds can be directly integrated into conventional oxide heterostructures and, therefore, investigated using state-of-the-art growth and characterization techniques highly developed in the perovskite-oxide community.

In standard ABO_3 perovskites, the superexchange interaction is often antiferromagnetic (negative).[13] In B-site ordered DPs, instead, as summarized by the Goodenough, Kanamori, and Anderson rules,[14,15] the two distinct B and B' cations can be selected such that an empty d orbital of one 3d transition metal interacts with a half-filled 3d orbital of the other cation to produce a positive superexchange interaction. As this particular type of exchange is not mediated by conduction electrons, the resulting ferromagnetic order would naturally emerge within an insulating framework.

Among all the possible choices of A, B, and B' cations, a promising configuration is stabilized in La_2NiMnO_6 (LNMO). Bulk LNMO shows non-metallic behavior with a relatively high Curie

temperature (T_C) around 280 K.[16,17] It recently attracted further attention due to the discovery of some additional functionalities, such as colossal magnetodielectricity,[18] possible A-site driven ferroelectricity,[19] predicted multiferroicity in artificial superlattices,[20] or high-temperature paramagnetic spin pumping.[21] In view of the recent demand of FMIs for prospective spintronic applications, it seems timely to reinvestigate the properties of this compound in thin films. Previous reports have shown that pulsed laser deposition,[22–24] molecular beam epitaxy,[25] and polymer-assisted chemical deposition[26] can be suitable growth methods to produce LNMO thin films. Despite that, to our knowledge, there are no reports showing the stabilization of a two-dimensional growth mode, a prerequisite for any possible implementation of LNMO thin films in a multi-layer device architecture.

In the following, we will show that atomically precise B-site ordered LNMO films can be deposited by off-axis radio-frequency

(RF) magnetron sputtering on a variety of oxide substrates inducing both compressive and tensile strain. We find that their near room temperature T_C is independent of epitaxial strain while the films retain insulating transport properties. These results suggest that the magnetic interaction between Ni and Mn in the LNMO system is pretty robust against structural changes and thus suitable for a variety of spintronic devices where a high-temperature FM insulating state is essential.

II. STRUCTURAL AND ELECTRONIC PROPERTIES

LNMO films were epitaxially grown on (001)-oriented LaAlO₃ (LAO), $(LaAlO_3)_{0.3}(SrAl_{0.5}Ta_{0.5}O_3)_{0.7}$ (LSAT), SrTiO₃ (STO) and (110)-oriented NdGaO₃ (NGO), LaGaO₃ (LGO), and DyScO₃ (DSO) substrates. The films were grown using off-axis RF magnetron sputtering at a substrate temperature of 720 °C and a total pressure of 0.18 mbar in a controlled mixture of oxygen and argon. Additional details on both the growth and characterization methods are discussed in the supplementary material.

Assuming a pseudocubic (pc) lattice constant of LNMO of 3.876 Å (a value obtained by averaging the characteristic lattice constant of the two room-temperature LNMO polymorphs, rhombohedral and monoclinic[27]), a compressive strain of −2.1%, −0.5%, and −0.2% on LAO, NGO, and LSAT and a tensile strain of +0.4%, +0.7%, and +1.8% on LGO, STO, and DSO substrates, respectively, are imposed. X-ray diffraction (XRD) θ–2θ scans around the pc (001) diffraction plane of the aforementioned substrates is shown in Fig. 1(b) and highlights the crystalline quality of our sputter-grown films. From the fringes in the XRD data, we confirmed that the thickness of our strained films is in the order of 30 pc unit cells (uc), ≈12 nm, as expected from previous growth calibrations. All six films are fully strained to the substrate in-plane lattice constant as observed in the reciprocal space maps measured around the (103)pc diffraction condition of the respective substrates [Fig. 1(c) for LNMO//STO and Fig. S1 for a selection of other strained films].

In the top panel of Fig. 1(d), we present the surface topography of a representative LNMO//STO film imaged by atomic force microscopy (AFM). Atomic steps inherited from the underlying substrate topography suggest the stabilization of a two-dimensional growth mode. Similar step-and-terrace morphology is also obtained for films grown on LSAT, NGO, LGO, and DSO, while the topography of a LNMO//LAO film is characterized by island growth (not shown). This can be tentatively attributed to the large compressive strain exerted by the substrate that might require substrate-specific growth optimizations.[28] The two-dimensional growth mode of the LNMO//STO heterostructure is further corroborated by the streaky reflection high-energy electron diffraction (RHEED) pattern obtained after the growth [bottom panels of Fig. 1(d)] and by the intensity oscillations of the *in situ* RHEED specular spot [inset of the top panel in Fig. 1(d)] that are typically associated with a layer-by-layer growth mode.[29] The complete intensity profile is reported in Fig. S2 of the supplementary material. To perform RHEED in our sputtering chamber, we employ the same gun configuration described by Podkaminer *et al.* for the first time demonstration of the layer-by-layer growth control during sputter deposition.[30]

In Fig. 1(e), we show a high-angle annular dark-field scanning transmission electron microscopy (HAADF-STEM) image of a LNMO//STO film collected along the $[100]_{STO}$ zone axis that highlights the absence of both dislocations and undesired parasitic phases. Similar results were obtained along the $[110]_{STO}$ zone axis. The additional HAADF-STEM images are provided in Fig. S3. The stoichiometry of our films was verified using both Rutherford backscattering (RBS) and x-ray photoemission spectroscopy (XPS), as discussed in more detail in the supplementary material.

The evidence of correct stoichiometry, however, is not enough to determine the presence of cation ordering. To validate that our LNMO films are not a solid solution but rather formed by a rock-salt arrangement of the NiO₆ and MnO₆ octahedra, we acquired energy dispersive x-ray (EDX) spectrum images along the $[110]_{STO}$ zone axis. These are presented in Fig. 1(f). The elemental maps calculated from the EDX spectrum image reveal a good Ni–Mn rock-salt ordering over the whole LNMO film. The complete set of EDX elemental maps and the corresponding extracted line profiles are shown in Fig. S4 of the supplementary material.

To further corroborate the presence of long-range B-cation ordering, we also performed XRD along the $[111]_{pc}$ direction. To improve the signal-to-noise ratio of our in-house diffractometer, we performed the scan on a thicker film of 90 uc (≈35 nm) grown on a (001)-oriented STO substrate [Fig. 2(a)]. The same measurement for a bare STO substrate is also displayed for comparison. As a direct consequence of the rock-salt ordering of the B and B′ cations forming the DP cell, a new periodicity along $(\frac{1}{2}, \frac{1}{2}, \frac{1}{2})_{pc}$ emerges in our film, which confirms the long-range order of Mn and Ni cations in our sputter-grown LNMO thin films.[31] With the aid of selection rules,[32] we can exclude that this diffraction peak emerges from the octahedra tilt system of LNMO.

It has been observed, however, that the origin of these half-order superstructures in DPs could also occur due to unequal A-cation displacement along the $[111]_{pc}$ direction, mimicking the unit cell of the chemically ordered compound.[19,33] As the chemical ordering in LNMO bulk specimens is accompanied by an electronic charge transfer from the nominally Ni³⁺ ions to the nominally Mn³⁺ ions culminating in a Ni²⁺/Mn⁴⁺ electronic configuration,[18,34] the observation of this charge transfer can also be considered a landmark of the rock-salt ordering of the NiO₆ and MnO₆ octahedra forming the DP structure.[16]

To access the electronic configuration of Ni and Mn, we performed x-ray absorption spectroscopy (XAS) measurements in the soft x-ray regime at the X-Treme beamline (SLS-PSI),[35] as this technique is strongly sensitive to the valence state of the probed transition-metal ion.[36] In the top panels of Figs. 2(b) and 2(c), we present the XAS collected at the Mn (Ni) L₂,₃ edges in the total electron yield (TEY) for the whole set of epitaxially strained films, while in the bottom panels, we show the associated reference spectra. A comparison between the LNMO spectra and the references indicates that the Mn prevalently adopts a 4+ configuration, while the Ni is in a 2+ state. This can be deduced from two specific features: first, the position of the Mn L₃-edge pre-peak around 639.5 eV corresponds to the one of SrMnO₃ (Mn⁴⁺); second, the multiplet structure of the Ni L₂-edge around 870 eV is strongly reminiscent of the one measured in NiO (Ni²⁺). Concerning the residual differences in the XAS spectra between the DP LNMO Mn⁴⁺ and the single perovskite
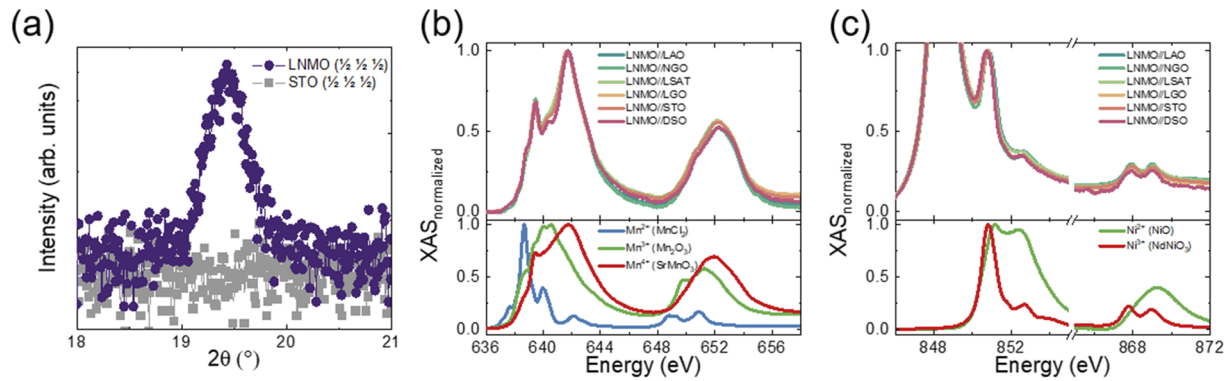
FIG. 2. B-cation ordering. (a) XRD collected along the $(111)_{pc}$ plane of a 90 uc LNMO//STO film (purple circles) and a representative STO substrate (gray squares). The half-order peak emerges due to the three-dimensional B/B′-cation-ordering of the DP structure. (b) Top: XAS data collected at 300 K in the TEY mode at the Mn $L_{2,3}$-edges for the whole set of 30 uc epitaxially strained LNMO films normalized to the L_3-edge maximum. Bottom: reference Mn spectra. (c) Same as (b) collected at the Ni $L_{2,3}$-edges. The out-of-scale peak around 848.5 eV corresponds to the La M_4 absorption edge. The comparison between top and bottom panels certifies the prevalence of both Mn^{4+} and Ni^{2+} valence configurations, as discussed in the main text.

reference Mn^{4+}, these have been already investigated in bulk specimens and attributed to the different local geometry of the Ni and Mn cations, resulting in a distinct crystal field environment.[37] Albeit we cannot exclude that a small portion of Mn ions adopts a 3+ configuration in the LNMO films grown on LSAT and STO, a thorough characterization that is going to be discussed in future work indicates that this effect has an interfacial origin and is not related to epitaxial strain and/or growth conditions. Thus, our epitaxially strained LNMO films grown by off-axis RF magnetron sputtering are stoichiometric and with a cation-ordered DP structure.

Finally, we note that all the films display high resistivity (≈ 1 kΩ cm) at room temperature independently of their strain state. We were unable to measure the temperature-dependence of the resistivity in our physical property measurement system because it

was always lying above our measurement limit, confirming that the insulating-like transport properties of the films are consistent with bulk characterization.[17]

III. MAGNETIC PROPERTIES

After having determined the structural and electronic properties of our LNMO films, we now investigate their magnetic properties. We present in Fig. 3(a) the hysteresis loop of a 30 uc LNMO//STO film measured at 5 K by superconducting quantum interference device (SQUID) magnetometry. Special care was taken to remove the STO substrate magnetic contributions.[38] The film is characterized by a saturation magnetization of 4.3 μ_B/f.u., comparable with other high-quality bulk specimens.[39,40] We also observe
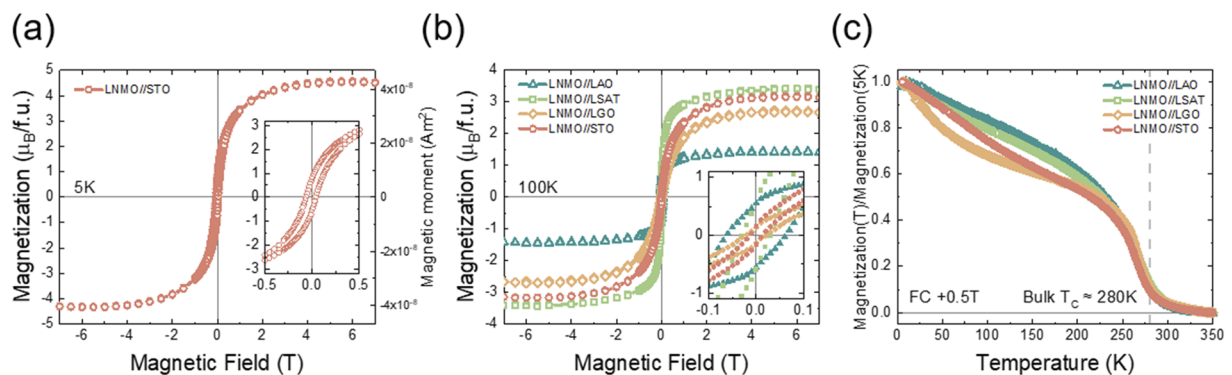
FIG. 3. Magnetic properties investigated by SQUID magnetometry. (a) Isothermal magnetization curve collected at 5 K for a 30 uc LNMO//STO film. We observe a saturation magnetization of 4.3 μ_B/f.u. (magnetic moment of 4.2×10^{-8} A m^2). Inset: closer view of the opening of the hysteresis loop. (b) Magnetization curve collected at 100 K for films of 30 uc grown on LAO, LSAT, LGO, and STO. The film grown on LAO, subjected to a larger epitaxial strain, is characterized by a lower in-plane saturation magnetization. The inset shows that, together with the hysteresis opening, we also observe a slightly larger coercive field for increasing compressive epitaxial strain. (c) The magnetization as a function of the temperature normalized to the 5 K value indicates similar Curie temperatures for different LNMO films, independent of their epitaxial strain. The bulk T_C is highlighted with a dashed line. The data are collected during field cooling (FC) in an in-plane magnetic field of $+0.5$ T.

a coercive field in the order of 300 Oe and a low remnant magnetization (<1 μ_B/f.u.), again in accordance with values reported in the literature.[16,17] A higher remnant magnetization ($\gtrsim 1$ μ_B/f.u.) can, instead, be associated with an excess of Mn,[16] and it should be considered a warning for non-stoichiometric films.[22,26,31,41] The low remanence has been previously attributed to the presence of long-range ordered FM domains that, in stoichiometric films, are coupled antiferromagnetically across antiphase boundaries,[16] a characteristic that LNMO shares with other magnetically ordered DPs.[42] Nevertheless, in our 10-μm-wide lamellae prepared for STEM imaging, we could not detect any antiphase domains, suggesting that their average size in our epitaxially strained films could be potentially larger than 10 μm.

In Fig. 3(b), we compare the hysteresis loops collected at 100 K for some of the differently strained samples. We explored this temperature to minimize the low-temperature magnetic contributions arising from the substrates. The strong paramagnetic signal of both NGO and DSO substrates excludes the possibility of using SQUID magnetometry to characterize the magnetic properties of the associated LNMO films; still, films grown on LSAT, LGO, and STO seem to have similar saturation magnetization around 3 μ_B/f.u. at 100 K, whereas the film grown on LAO has a lower saturation magnetization. We also observe a small trend of increasing coercive field as compressive strain increases [inset of Fig. 3(b)]. This preliminarily be associated with a hardening of the in-plane magnetic axis induced by epitaxial strain.[43,44] Finally, in Fig. 3(c), we compare the temperature-dependent magnetization normalized to its 5 K value for the films shown in Fig. 3(b). We find that, despite the different saturation magnetizations, the LNMO films are always characterized by a T_C around 280 K accompanied by a non-zero magnetization tail at higher temperatures,[45–47] to which we will come back shortly. This remarkable stability against epitaxial strain corroborates a similar result obtained in bulk specimens using hydrostatic pressure.[48]

and further suggests a prospective use of LNMO films for spintronic applications.

To further characterize the magnetism of the strained films, we performed x-ray magnetic circular dichroism (XMCD) measurements. Due to the insulating nature of both films and substrates, we observe a strong charging at low temperatures promoted by the synchrotron radiation in the data collected in TEY. Only the films grown on STO seem to be less affected by this issue, probably due to the innate ability of this substrate to transport charge carriers.[49] At the Ni $L_{2,3}$-edge, this obstacle can be overcome by measuring in the total fluorescence yield (TFY). Unfortunately, this is not the case for the Mn edges due to the dominant role of self-absorption[50] caused by the proximity to the O K-edge.[51] Consequently, we show in Fig. 4(a) the dichroism measured at 100 K and 5 T at the Mn $L_{2,3}$-edges in the TEY mode for the LNMO//STO sample (top panel) and at the Ni $L_{2,3}$-edges in the TFY mode for all strained films (bottom panel). From the concordant sign of the XMCD measured at both edges, we confirm the expected ferromagnetic coupling of the Ni and Mn sublattices.[52] To determine a trend as a function of strain, in the inset of Fig. 4(a), we display the integral calculated over the Ni L_3-edge subtracted by two times the integral calculated over the Ni L_2-edge (i.e., L_3-2 $\times$ L_2). This quantity is proportional to the numerator in the spin sum rule[53] and is therefore directly related to the magnetization of our films. We resort to this strategy because the integral of the XAS (the denominator in the spin sum rule) is hard to determine due to the presence of the lanthanum M_4 absorption edge. Despite this limitation, we derive that the saturation magnetization of the LNMO films decreases as either compressive or tensile strain increases, in agreement with our previous observation by SQUID magnetometry. To understand this occurrence, it is useful to recall that perovskite films can accommodate epitaxial strain also with vacancies' formation.[54,55] It is plausible, therefore, that such reduced structural stability could result in an increased
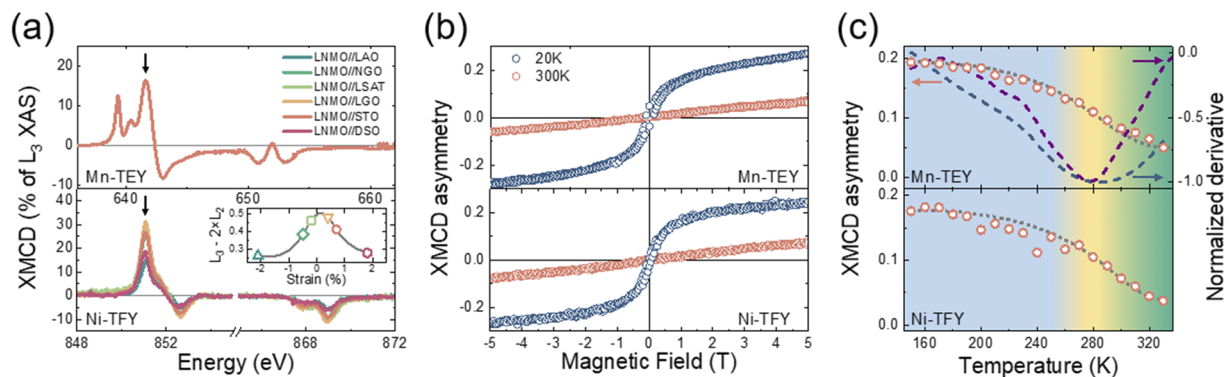
FIG. 4. Magnetic properties investigated by synchrotron radiation. (a) In the top (bottom) panel, the XMCD data collected at the Mn (Ni) $L_{2,3}$-edges at 100 K for a LNMO//STO film in the TEY (TFY) mode are displayed. For the Ni $L_{2,3}$-edges, all the other strained films are also shown (see main text). Black arrows indicate the resonant energy chosen to calculate the asymmetry. In the inset, the L_3-2 $\times$ L_2 integral calculated over the Ni $L_{2,3}$-edges is shown, with the gray line being a guide to the eye. (b) In the top (bottom) panel, XMCD asymmetry of Mn (Ni) as a function of the magnetic field measured at 20 K (blue circles) and 300 K (red circles) for the LNMO//STO film is displayed. (c) In the top (bottom) panel, XMCD asymmetry of Mn (Ni) as a function of the sample temperature measured in a magnetic field of 5 T (red circles) is displayed. The gray dotted line is a guide to the eye. Dashed lines indicate the derivative of XMCD asymmetry (blue) and SQUID (purple) data measured using the same external magnetic field. The transition interval (yellow) from the ferromagnetic (light blue) to the paramagnetic phase (green) is chosen to be around the minimum of the derivatives. Colored arrows indicate the respective axes.

antisite disorder for larger strains, leading to additional anti-ferromagnetic interactions via the $Mn^{4+}–O^{2-}–Mn^{4+}$ and $Ni^{2+}–O^{2-}–Ni^{2+}$ bonds.[16,39,56] Note that if the antisite disorder is randomly distributed in the whole film volume, we do not expect the appearance of exchange bias, the absence of which can, indeed, be observed in the inset of Fig. 3(b). The resulting lowering of the saturation magnetization, however, is not correlated with a reduction of the Curie temperature,[39] as shown in Fig. 3(c), again remarking the impressive stability of the $Mn^{4+}–O^{2-}–Ni^{2+}$ ferromagnetic superexchange interaction.[48,57]

With XMCD, we can also follow the element-specific evolution of the magnetization as a function of the external magnetic field. In particular, we plot in Fig. 4(b) the XMCD asymmetry defined as the maximum XMCD contrast measured with left or right polarization at the energies indicated by the small arrows in Fig. 4(a). The magnetic response of the Mn and Ni sublattices is similar, confirming that despite the DP unit cell being formed by two distinct transition metal ions, it behaves as if featuring a single magnetic sublattice. Moreover, while the asymmetry ratio measured at 20 K tends to saturate, a clear linear paramagnetic shape is observed at 300 K. This suggests that the room-temperature magnetic moment measured by SQUID [Fig. 3(c)] is not due to ferromagnetic ordering but must be attributed to short-range magnetic correlations, as already extensively discussed in the available literature.[45,47,58]

Finally, to present a complementary way to determine T_C, we show in Fig. 4(c) the XMCD asymmetry of the same LNMO//STO sample collected with a field of 5 T as a function of the temperature. We use a strong external field to saturate the magnetization and to maximize the signal-to-noise ratio, but, as a consequence, the ferromagnetic–paramagnetic phase transition is smeared out due to the field effect. To determine the transition temperature, we calculate the derivative of the XMCD asymmetry and we fix T_C to be its minimum. The Curie temperature derived in this way is located slightly above 280 K. Using the same derivative approach to analyze the SQUID magnetometry data[59] collected in a field of 5 T, we find a T_C around 275 K. Both these numbers are in agreement with the reported bulk values[16,17] and thus corroborate the use of temperature-dependent XMCD to investigate magnetic phase transitions.[60,61]

IV. SUMMARY AND CONCLUSIONS

We have shown that off-axis RF magnetron sputtering is a suitable growth method to produce atomically precise, stoichiometric, and cation-ordered LNMO thin films. We find that our films are characterized by an insulating behavior paired with a T_C in the order of 280 K, independent of epitaxial strain. We further observe that films subjected to lower epitaxial strain possess a larger saturation magnetization. XMCD hysteresis loops and thermal asymmetry collected at both the Mn and Ni edges further clarify the paramagnetic nature of the LNMO films at room temperature. Our observations confirm that the non-zero magnetization observed at 300 K in this compound must be attributed to the presence of short-range correlations.[45] Importantly, these can still be exploited in potential applications where interfacial effects are dominant.[21] Considering the scarcity of ferromagnetic perovskite oxides with high T_C and non-metallic transport properties, we anticipate that LNMO thin films can act both as an optimal platform for fundamental studies in the oxide electronics community and as candidate material for prospective applications in spintronic devices.

SUPPLEMENTARY MATERIAL

See the supplementary material for the experimental details on the growth methods and characterization and the determination of cation stoichiometry using RBS and XPS.

DATA AVAILABILITY

The data that support the findings of this study are available from the corresponding author upon reasonable request.

REFERENCES

[1]G. E. W. Bauer, E. Saitoh, and B. J. van Wees, Nat. Mater. **11**, 391 (2012).

[2]A. V. Chumak, V. I. Vasyuchka, A. A. Serga, and B. Hillebrands, Nat. Phys. **11**, 453 (2015).

[3]M. Coll, J. Fontcuberta, M. Althammer, M. Bibes, H. Boschker, A. Calleja, G. Cheng, M. Cuoco, R. Dittmann, B. Dkhil, I. El Baggari, M. Fanciulli, I. Fina, E. Fortunato, C. Frontera, S. Fujita, V. Garcia, S. T. B. Goennenwein, C.-G. Granqvist, J. Grollier, R. Gross, A. Hagfeldt, G. Herranz, K. Hono, E. Houwman, M. Huijben, A. Kalaboukhov, D. J. Keeble, G. Koster, L. F. Kourkoutis, J. Levy, M. Lira-Cantu, J. L. MacManus-Driscoll, J. Mannhart, R. Martins, S. Menzel, T. Mikolajick, M. Napari, M. D. Nguyen, G. Niklasson, C. Paillard, S. Panigrahi, G. Rijnders, F. Sánchez, P. Sanchis, S. Sanna, D. G. Schlom, U. Schroeder, K. M. Shen, A. Siemon, M. Spreitzer, H. Sukegawa, R. Tamayo, J. van den Brink, N. Pryds, and F. M. Granozio, Appl. Surf. Sci. **482**, 1 (2019).

[4]C. Zener, Phys. Rev. **82**, 403 (1951).

[5]P. Zubko, S. Gariglio, M. Gabay, P. Ghosez, and J.-M. Triscone, Annu. Rev. Condens. Matter Phys. **2**, 141 (2011).

[6]D. I. Khomskii, *Transition Metal Compounds* (Cambridge University Press, Cambridge, 2014).

[7]H. Boschker, J. Kautz, E. P. Houwman, W. Siemons, D. H. A. Blank, M. Huijben, G. Koster, A. Vailionis, and G. Rijnders, Phys. Rev. Lett. **109**, 157207 (2012).

[8]D. Meng, H. Guo, Z. Cui, C. Ma, J. Zhao, J. Lu, H. Xu, Z. Wang, X. Hu, Z. Fu, R. Peng, J. Guo, X. Zhai, G. J. Brown, R. Knize, and Y. Lu, Proc. Natl. Acad. Sci. U. S. A. **115**, 2873 (2018).

[9]C. Sohn, E. Skoropata, Y. Choi, X. Gao, A. Rastogi, A. Huon, M. A. McGuire, L. Nuckols, Y. Zhang, J. W. Freeland, D. Haskel, and H. N. Lee, Adv. Mater. **31**, 1805389 (2019).

[10]W. Li, B. Zhu, Q. He, A. Y. Borisevich, C. Yun, R. Wu, P. Lu, Z. Qi, Q. Wang, A. Chen, H. Wang, S. A. Cavill, K. H. L. Zhang, and J. L. MacManus-Driscoll, Adv. Sci. **7**, 1901606 (2020).

[11]Y. Wang, Q. He, W. Ming, M. H. Du, N. Lu, C. Cafolla, J. Fujioka, Q. Zhang, D. Zhang, S. Shen, Y. Lyu, A. T. N'diaye, E. Arenholz, L. Gu, C. Nan, Y. Tokura, S. Okamoto, and P. Yu, Phys. Rev. X **10**, 021030 (2020).

[12]S. Vasala and M. Karppinen, Prog. Solid State Chem. **43**, 1 (2015).

[13]P. W. Anderson, Phys. Rev. **79**, 350 (1950).

[14]J. B. Goodenough, Phys. Rev. **100**, 564 (1955).

[15]J. Kanamori, J. Phys. Chem. Solids **10**, 87 (1959).

[16]R. I. Dass, J.-Q. Yan, and J. B. Goodenough, Phys. Rev. B **68**, 064415 (2003).

[17]N. S. Rogado, J. Li, A. W. Sleight, and M. A. Subramanian, Adv. Mater. **17**, 2225 (2005).

[18]D. Choudhury, P. Mandal, R. Mathieu, A. Hazarika, S. Rajan, A. Sundaresan, U. V. Waghmare, R. Knut, O. Karis, P. Nordblad, and D. D. Sarma, Phys. Rev. Lett. **108**, 127201 (2012).

[19]R. Takahashi, I. Ohkubo, K. Yamauchi, M. Kitamura, Y. Sakurai, M. Oshima, T. Oguchi, Y. Cho, and M. Lippmaa, Phys. Rev. B **91**, 134107 (2015).

[20]H. J. Zhao, W. Ren, Y. Yang, J. Íñiguez, X. M. Chen, and L. Bellaiche, Nat. Commun. **5**, 4021 (2014).

[21]Y. Shiomi and E. Saitoh, Phys. Rev. Lett. **113**, 266602 (2014).

[22]H. Z. Guo, J. Burgess, E. Ada, S. Street, A. Gupta, M. N. Iliev, A. J. Kellock, C. Magen, M. Varela, and S. J. Pennycook, Phys. Rev. B **77**, 174423 (2008).

[23]M. Kitamura, I. Ohkubo, M. Kubota, Y. Matsumoto, H. Koinuma, and M. Oshima, Appl. Phys. Lett. **94**, 132506 (2009).

[24]S.-Q. Wu, S. Cheng, L. Lu, M. Liu, X.-W. Jin, S.-D. Cheng, and S.-B. Mi, Sci. Rep. **8**, 2516 (2018).

[25]S. R. Spurgeon, Y. Du, T. Droubay, A. Devaraj, X. Sang, P. Longo, P. Yan, P. G. Kotula, V. Shutthanandan, M. E. Bowden, J. M. LeBeau, C. Wang, P. V. Sushko, and S. A. Chambers, Chem. Mater. **28**, 3814 (2016).

[26]H. Wang, C. Frontera, J. Herrero-Martín, A. Pomar, P. Roura, B. Martínez, and N. Mestres, Chem.-Eur. J. **26**, 9338 (2020).

[27]C. L. Bull, D. Gleeson, and K. S. Knight, J. Phys.: Condens. Matter **15**, 4927 (2003).

[28]Y. Sakurai, I. Ohkubo, Y. Matsumoto, H. Koinuma, and M. Oshima, J. Appl. Phys. **110**, 063913 (2011).

[29]G. J. H. M. Rijnders, G. Koster, D. H. A. Blank, and H. Rogalla, Appl. Phys. Lett. **70**, 1888 (1997).

[30]J. P. Podkaminer, J. J. Patzner, B. A. Davidson, and C. B. Eom, APL Mater. **4**, 086111 (2016).

[31]M. P. Singh, K. D. Truong, S. Jandl, and P. Fournier, Phys. Rev. B **79**, 224421 (2009).

[32]D. I. Woodward and I. M. Reaney, Acta Crystallogr., Sect. B: Struct. Sci. **61**, 387 (2005).

[33]V. Shabadi, M. Major, P. Komissinskiy, M. Vafaee, A. Radetinac, M. Baghaie Yazdi, W. Donner, and L. Alff, J. Appl. Phys. **116**, 114901 (2014).

[34]G. Blasse, J. Inorg. Nucl. Chem. **27**, 993 (1965).

[35]C. Piamonteze, U. Flechsig, S. Rusponi, J. Dreiser, J. Heidler, M. Schmidt, R. Wetter, M. Calvi, T. Schmidt, H. Pruchova, J. Krempasky, C. Quitmann, H. Brune, and F. Nolting, J. Synchrotron Radiat. **19**, 661 (2012).

[36]M. Abbate, F. M. F. de Groot, J. C. Fuggle, A. Fujimori, O. Strebel, F. Lopez, M. Domke, G. Kaindl, G. A. Sawatzky, M. Takano, Y. Takeda, H. Eisaki, and S. Uchida, Phys. Rev. B **46**, 4511 (1992).

[37]M. C. Sánchez, J. García, J. Blasco, G. Subías, and J. Perez-Cacho, Phys. Rev. B **65**, 144409 (2002).

[38]J. M. D. Coey, M. Venkatesan, and P. Stamenov, J. Phys.: Condens. Matter **28**, 485001 (2016).

[39]S. Pal, S. Govinda, M. Goyal, S. Mukherjee, B. Pal, R. Saha, A. Sundaresan, S. Jana, O. Karis, J. W. Freeland, and D. D. Sarma, Phys. Rev. B **97**, 165137 (2018).

[40]C. J. Ridley, D. Daisenberger, C. W. Wilson, G. B. G. Stenning, G. Sankar, K. S. Knight, M. G. Tucker, R. I. Smith, and C. L. Bull, Inorg. Chem. **58**, 9016 (2019).

[41]M. Bernal-Salamanca, Z. Konstantinović, L. Balcells, E. Pannunzio-Miner, F. Sandiumenge, L. Lopez-Mir, B. Bozzo, J. Herrero-Martín, A. Pomar, C. Frontera, and B. Martínez, Cryst. Growth Des. **19**, 2765 (2019).

[42]J. B. Goodenough and R. I. Dass, Int. J. Inorg. Mater. **2**, 3 (2000).

[43]R. Galceran, L. López-Mir, B. Bozzo, J. Cisneros-Fernández, J. Santiso, L. Balcells, C. Frontera, and B. Martínez, Phys. Rev. B **93**, 144417 (2016).

[44]C. Du, R. Adur, H. Wang, A. J. Hauser, F. Yang, and P. C. Hammel, Phys. Rev. Lett. **110**, 147204 (2013).

[45]S. Zhou, L. Shi, H. Yang, and J. Zhao, Appl. Phys. Lett. **91**, 172505 (2007).

[46]H. Guo, A. Gupta, M. Varela, S. Pennycook, and J. Zhang, Phys. Rev. B **79**, 172402 (2009).

[47]S. M. Zhou, Y. Q. Guo, J. Y. Zhao, S. Y. Zhao, and L. Shi, Appl. Phys. Lett. **96**, 262507 (2010).

[48]D. Haskel, G. Fabbris, N. M. Souza-Neto, M. van Veenendaal, G. Shen, A. E. Smith, and M. A. Subramanian, Phys. Rev. B **84**, 100403(R) (2011).

[49]R. Moos, W. Menesklou, and K. H. Härdtl, Appl. Phys. A: Mater. Sci. Process. **61**, 389 (1995).

[50]H. Wadati, A. J. Achkar, D. G. Hawthorn, T. Z. Regier, M. P. Singh, K. D. Truong, P. Fournier, G. Chen, T. Mizokawa, and G. A. Sawatzky, Appl. Phys. Lett. **100**, 193906 (2012).

[51]F. M. F. De Groot, Nat. Chem. **4**, 766 (2012).

[52]J. Blasco, J. García, M. C. Sánchez, J. Campo, G. Subías, and J. Pérez-Cacho, Eur. Phys. J. B **30**, 469 (2002).

[53]C. Piamonteze, P. Miedema, and F. M. F. de Groot, Phys. Rev. B **80**, 184410 (2009).

[54]U. Aschauer, R. Pfenninger, S. M. Selbach, T. Grande, and N. A. Spaldin, Phys. Rev. B **88**, 054111 (2013).

[55]T. Grande, J. R. Tolchard, and S. M. Selbach, Chem. Mater. **24**, 338 (2012).

[56]J. B. de Azevedo Filho, R. F. Souza, J. C. A. Queiroz, T. H. C. Costa, C. P. S. Sena, S. G. C. Fonseca, A. O. da Silva, and J. B. L. Oliveira, J. Magn. Magn. Mater. **527**, 167770 (2021).

[57]P. Sanyal, Phys. Rev. B **96**, 214407 (2017).

[58]M. N. Iliev, H. Guo, and A. Gupta, Appl. Phys. Lett. **90**, 151914 (2007).

[59]Y. Xie, J. Fan, L. Xu, X. Zhang, R. Xu, Y. Zhu, R. Tang, C. Wang, C. Ma, L. Pi, Y. Zhang, and H. Yang, Phys. Lett. A **383**, 125843 (2019).

[60]C. Stamm, J.-U. Thiele, T. Kachel, I. Radu, P. Ramm, M. Kosuth, J. Minár, H. Ebert, H. A. Dürr, W. Eberhardt, and C. H. Back, Phys. Rev. B **77**, 184401 (2008).

[61]H. Yibole, F. Guillou, L. Caron, E. Jiménez, F. M. F. de Groot, P. Roy, R. de Groot, N. H. van Dijk, and E. Brück, Phys. Rev. B **91**, 014429 (2015).